Digest Journal of Nanomaterials and Biostructures

Dig. J. Nanomater. Bios. **2026**; 21(2): 55194
https://doi.org/10.31083/DJNB55194

Original Research

Microwave-Assisted Eco-Friendly Synthesis of Carbon Quantum Dots With High Fluorescence Quantum Yields

Salma Aziz Neamah[1], Mundher Al-Shakban[2,*], Sattar M. Hassan[3], Zahraa Majid Hammoud[4]

[1]The General Directorate of Misan Education, Ministry of Education, 62001 Misan, Iraq
[2]Department of Physics, College of Science, University of Misan, 62001 Misan, Iraq
[3]Department of Mathematics, College of Education, University of Misan, 62001 Misan, Iraq
[4]Department of Chemistry, College of Science, University of Misan, 62001 Misan, Iraq
*Correspondence: Mundher.Al-Shakban@uomisan.edu.iq (Mundher Al-Shakban)
Academic Editor: Reshef Tenne
Submitted: 18 September 2025 Revised: 15 December 2025 Accepted: 23 December 2025 Published: 23 June 2026

Abstract

Carbon quantum dots (CQDs) luminescent carbon nanostructures are typically synthesized using complicated procedures and toxic reagents and feature insufficiently characterized structures. To address these limitations, we herein developed a simple and eco-friendly top-down microwave-assisted synthesis of CQDs from household supplies (sugar, vinegar, and baking soda). Ultraviolet–visible absorption spectroscopy, X-ray diffraction (XRD), and transmission electron microscopy (TEM) were used for CQD characterization. The average crystallite size of CQDs determined by XRD (50.627 ± 4 nm) reasonably well agreed with the average particle size determined by TEM (37 ± 5 nm), and the sample prepared under optimal conditions featured a fluorescence quantum yield of 0.247. Moreover, CQDs were shown to competitively inhibit lactate dehydrogenase.

Keywords: carbon quantum dots; photoluminescence; fluorescence; quantum yield

1. Introduction

Quantum dots semiconductor nanoparticles with diameters typically under 10 nm are widely used as markers and sensors, photodetectors, and display components because of their advantageous fluorescence properties [1,2] but typically contain heavy metals and are therefore toxic to humans and the environment [3]. Consequently, considerable attention has been drawn to carbon quantum dots (CQDs), which exhibit the fluorescence characteristics of conventional quantum dots but do not contain heavy metals and are therefore nontoxic and highly biocompatible [4].

The photophysical properties of quantum dots, including CQDs, are directly affected by their size and shape because of the quantum confinement effect [5], with smaller particles typically having a wider band gap (i.e., a larger energy difference between the lowest-energy conduction band and highest-energy valence band) [6]. As a result, quantum dots have higher emission efficiencies and excitation energies than their bulk counterparts. The fluorescence emission wavelength of quantum dots increases with their size [7]. The size of quantum dots is positively correlated with their fluorescence lifetime, e.g., electron–hole pairs in larger dots are confined within closer-spaced energy levels [8] and therefore have longer lifetimes [9]. A quantum dot, similar to a molecule, has a quantized density of electronic states close to the bandgap edge and a quantized energy spectrum. Correlations exist among the fluorescence lifetime, emission intensity, and shell thickness of quantum dots. A major advantage of quantum dots is the high degree of control over their size and hence, photophysical properties [10,11].

CQDs are nanoparticles that are primarily composed of carbon, typically have diameters of ≤10 nm, and exhibit fluorescence without necessarily displaying signs of quantum effects [12]. Owing to their advantageous fluorescence properties, high water solubility, stability, and functionalization simplicity, CQDs have attracted much attention and find numerous industrial (e.g., biomedicinal) applications [13]. However, CQDs are typically synthesized using complicated procedures and toxic reagents and have not been structurally characterized in detail. To address these limitations, we developed a simple and eco-friendly top-down microwave-assisted synthesis of CQDs, characterized them using ultraviolet–visible (UV–vis) absorption spectroscopy, X-ray diffraction (XRD), and transmission electron microscopy (TEM), and examined their ability to inhibit lactate dehydrogenase (LDH).

2. Materials and Methods

2.1 CQD Synthesis

Table sugar (sucrose), white vinegar (Aqueous acetic acid), and baking soda (sodium bicarbonate) were purchased from a local market in Misan, Iraq. A solution of table sugar (80 g) in distilled water (250 mL) was supplemented with white vinegar (100 mL) and microwaved in a microwave oven (ONAX, Model:DB) at medium heat (525

W) for 3 min. The resulting acidic solution of glucose and fructose was neutralized to pH 7.62 with baking soda (30.0 g) and then microwaved for two equal intervals (total heating time = 10, 13, or 16 min) to afford three CQD dispersions (samples A, B, and C, respectively).

2.2 CQD Characterization

TEM analysis (JEM-2100, JEOL, Tokyo, Japan) was performed by an external laboratory. UV–vis measurements were carried out in the 200–800 nm range using a UV-1800 spectrophotometer (Shimadzu, Kyoto, Japan). XRD analysis (Bruker AXS D8 Advance, Karlsruhe, Germany) was carried out using Cu K_α radiation (λ = 1.5406 Å). Fluorescence emission and excitation spectra were recorded using a spectrofluorophotometer (RF-5301 PC, Shimadzu, Kyoto, Japan).

LDH (BIOLABO SAS, Maizy, France) activity was estimated according to manufacturer's instructions using 80 mM Tris (pH 7.2) as a buffer, 1.6 mM pyruvate as a substrate, and 0.2 mM nicotinamide adenine dinucleotide (BIOLABO SAS, Maizy, France) as a coenzyme. LDH activity was defined as the enzyme quantity generating 1 µM of lactate per minute at 37 °C. Dilute CQD solutions (10, 15, 20, 25, and 50 ppm) were used as LDH inhibitors [14,15]. After incubating the substrate (1 mL) in a water bath at 37 °C for 5 min, the inhibitor (20 µL) and a pool of serum from individuals with hereditary hemolytic disorders (20 µL) were added. Absorbance was measured at 340 nm after 30 s, 1 min, and 2 min, and residual activity was determined as

$$\mathrm{UI/L} = \frac{\Delta\mathrm{Abs}}{\mathrm{min}} \times 8095 \quad (1)$$

where UI and ΔAbs are units of enzyme activity per liter and Change in absorbance per minute, respectively.

The percentage of inhibition was calculated as [16]

$$\%\ \mathrm{Inhibition} = \left(\frac{\mathrm{Activity}\frac{UI}{L}\ \text{with inhibitor}}{\mathrm{Activity}\frac{UI}{L}\ \text{without inhibitor}} \times 100\right) - 100 \quad (2)$$

3. Results

3.1 Photoluminescence

Solution color intensity increased with the increasing microwaving time (Fig. 1). All samples exhibited green fluorescence under 395-nm UV light (Fig. 2).

3.2 UV–Vis Analysis

Fig. 3 shows the UV–vis spectra of samples A–C and tryptophan (reference used for the subsequent determination of fluorescence quantum yield). For sample C, the spectrum showed saturation rather than a distinct absorption peak; therefore, no reliable absorption maximum was assigned, 267 nm (samples A and B), and 278 nm (tryptophan) and agreed with the fact that the deepest color was observed for sample C.

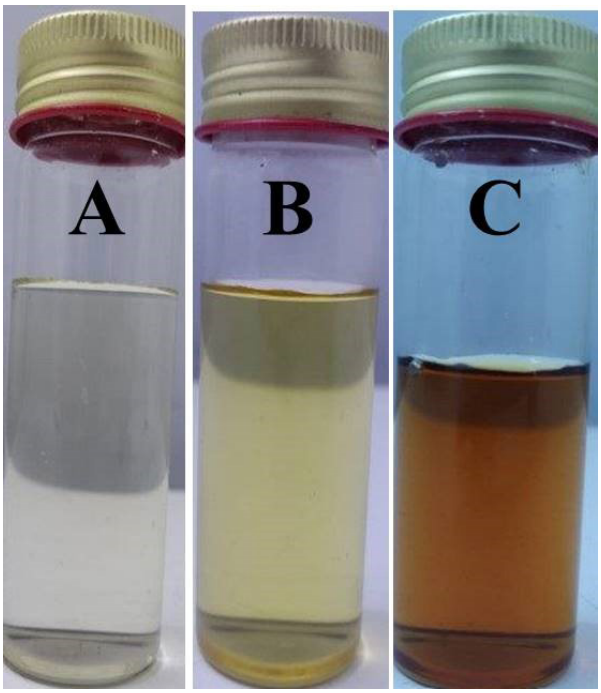

Fig. 1. Images of samples (A–C) under normal light.

3.3 Fluorescence Quantum Yield

To determine fluorescence quantum yields (Q values), measurements were performed for aqueous samples in the range of 300–900 nm using tryptophan as a reference.

$$Qs = Qr \times \frac{E_s A_r n_s^2}{E_r A_s n_r^2} \quad (3)$$

where n is the refractive index of the employed solvent, A is the solution absorbance at 278 nm, E is the integrated fluorescence intensity, and subscripts "r" and "s" denote the reference and unknown fluorophores, respectively. The $n_s{}^2/n_r{}^2$ ratio equals unity if the reference and unknown samples are dissolved in the same solvent, as in our case (solvent = water).

The determination of fluorescence quantum yields using the above method is based on the assumption that two solutions (reference and test sample) with the same absorbance at the excitation wavelength absorb the same number of photons.

The fluorescence spectra of tryptophan and the examined samples are provided in Figs. 4,5, respectively, and the corresponding fluorescence quantum yields are listed in Table 1 [17].

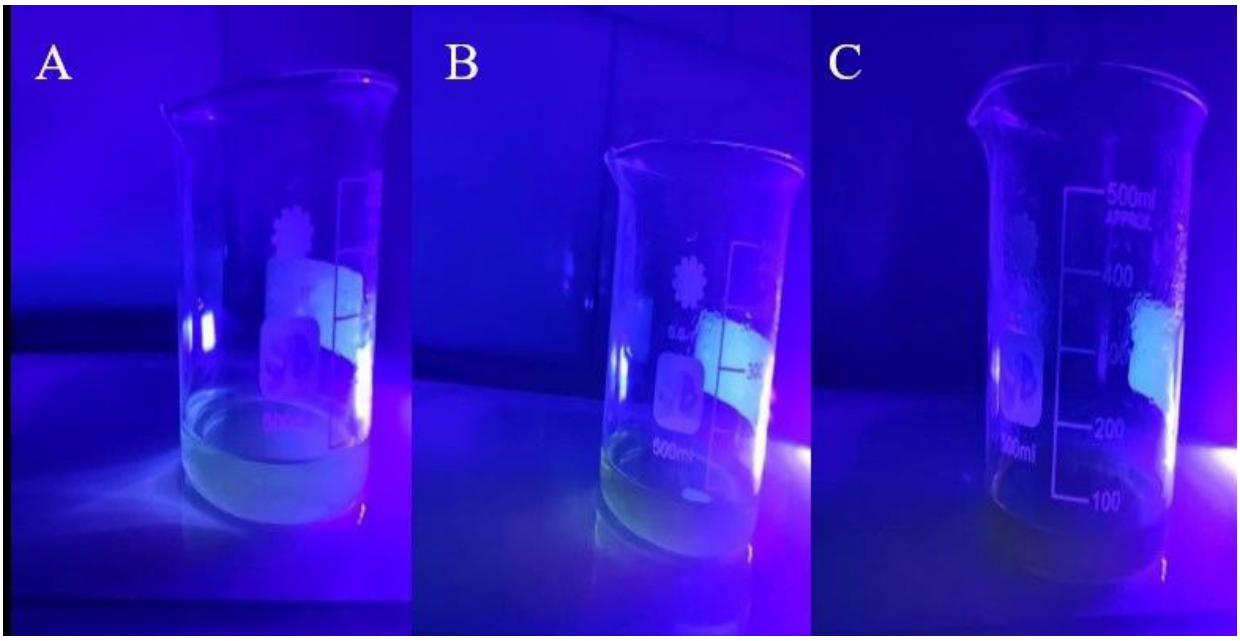

Fig. 2. Images of samples (A–C) under 395-nm ultraviolet (UV) light.

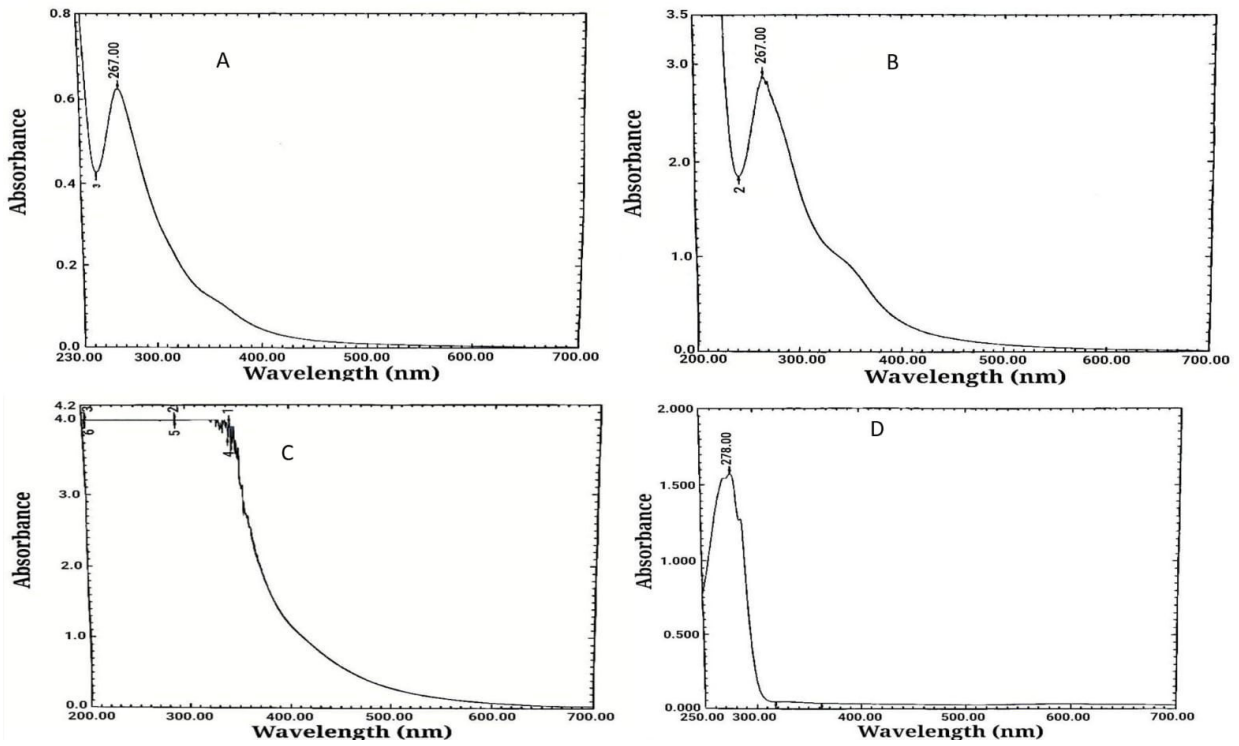

Fig. 3. Ultraviolet–visible (UV–vis) spectra of samples (A) A, (B) B, and (C) C and (D) tryptophan.

Table 1. Optical properties of samples A–C.

Compound	λ_{max} (nm)	A at 278 nm	Q
Tryptophan	278.00	1.576	0.15200
Sample A	267.00	0.600	0.24740
Sample B	267.00	2.900	0.11809
Sample C	354.50	4.000	0.09452

3.4 XRD Analysis

The XRD pattern of CQDs featured peaks at 2θ = 16.819°, 22.036°, 28.973°, 30.382°, 32.359°, 33.693°, 33.843°, 39.995°, 44.672°, 47.467°, 50.843°, and 57.793° (Fig. 6). The peak at 28.9735° was ascribed to the (002) plane of graphitic carbon (JCPDS No. 41-1487), confirming the presence of CQDs [18,19].

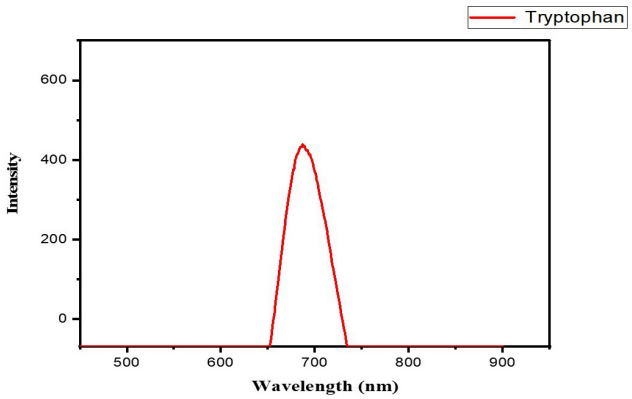

Fig. 4. Fluorescence spectrum of tryptophan.

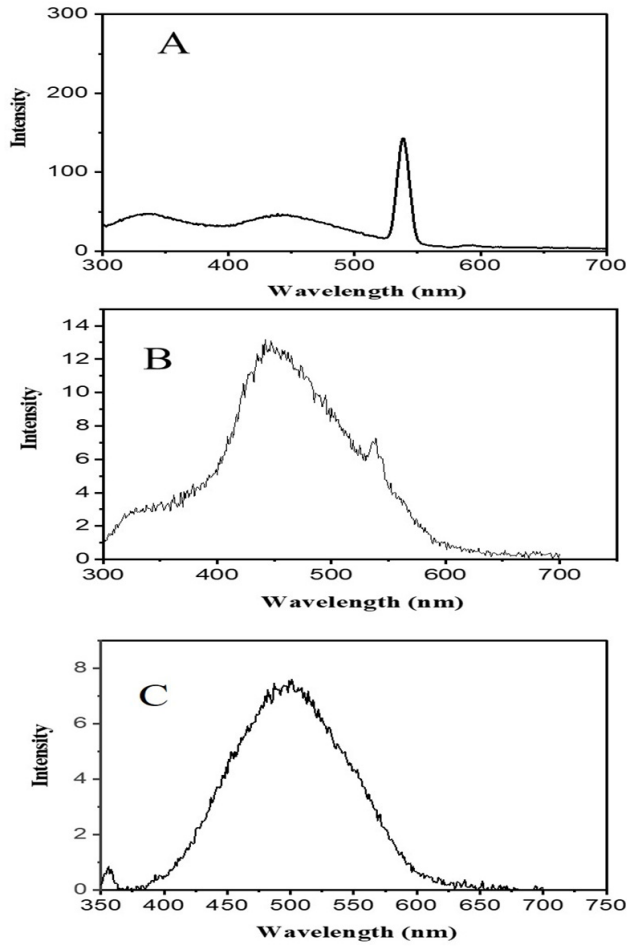

Fig. 5. Fluorescence spectra of samples (A–C).

Crystallite size D (nm) was determined using the Debye–Scherrer equation:

$$D = \frac{K\lambda}{\beta\cos\theta} \quad (4)$$

where $\lambda = 0.15406$ nm is the wavelength of X-ray radiation, β (rad) is the full width at half maximum of the peak of interest, θ (rad) is the Bragg (diffraction) angle of the peak of interest, and K is Constant [20] (Table 2).

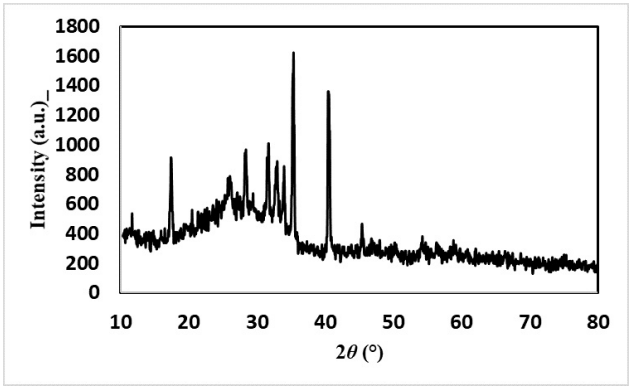

Fig. 6. X-ray diffraction (XRD) pattern of carbon quantum dots (CQDs).

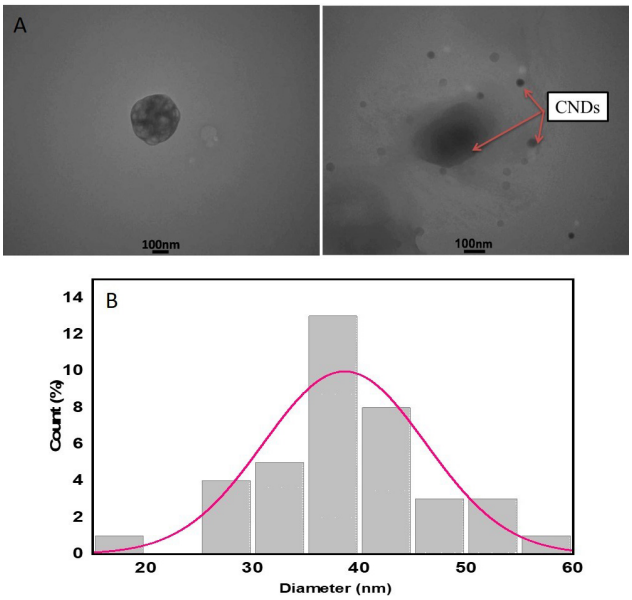

Fig. 7. Morphological characterization of CQDs. (A) TEM image and (B) size distribution of CQDs with a Gaussian fitting curve. TEM, Transmission Electron Microscopy; CNDs, Carbon Nanodots. Scale bar = 100 nm.

3.5 TEM Analysis

Fig. 7A shows representative TEM images of the CQDs, which appear as dark spheres free from contaminants. The only technique for measuring particle size that observes and measures individual particles directly is microscopy [21]. TEM images were processed using the ImageJ software to determine the CQD sizes and size distributions (Fig. 7B). The CQD size ranged from 10 to 70 nm, averaging to 37 ± 5 nm (n = 20).

Table 2. Crystallite sizes of CQDs calculated using different XRD peaks.

Peak position (2θ (°))	θ (°)	θ (rad)	cosθ	β [°2Th.]	β (rad)	D (nm)
16.8199	8.40995	0.1467	0.989	1.7698	0.0308	4.538
22.0366	11.01830	0.1922	0.981	0.4855	0.0084	16.672
28.9735	14.48675	0.2527	0.968	0.9192	0.0160	8.927
32.3596	16.17980	0.2822	0.960	0.7581	0.0132	10.912
33.6935	16.84675	0.2938	0.957	0.9840	0.0171	8.436
39.9958	19.99790	0.3488	0.939	0.3372	0.0058	25.072
44.6729	22.33645	0.3896	0.925	0.1732	0.0030	49.590
47.4674	23.73370	0.4140	0.915	1.3776	0.0240	6.299
50.8430	25.42150	0.4434	0.903	0.0900	0.0015	97.733
57.7930	28.89650	0.5040	0.875	0.0900	0.0015	101.038

Average D = 50.627 ± 4 nm.

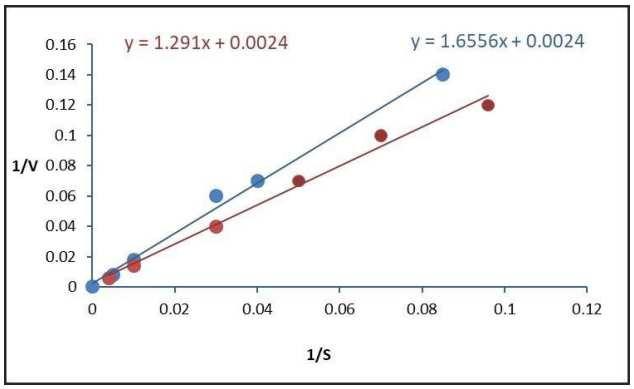

Fig. 8. Lineweaver–Burk plots obtained for lactate dehydrogenase in the presence and absence of CQDs.

3.6 Inhibitory Effect of CQDs on LDH

Fig. 8 presents Lineweaver–Burk plots for LDH obtained in the presence and absence of CQDs. Upon the introduction of CQDs, V_{max} (Maximum velocity) remained unchanged at 416.66 (µmol/min), whereas K_m (Michaelis constant) decreased from 689.822 to 537.90 (mM), which indicated competitive inhibition.

4. Discussion

Unlike previously reported CQD synthesis methods, ours uses simple and nontoxic/noncorrosive materials and household equipment and is energy-efficient. Under microwave irradiation, sucrose was hydrolyzed into glucose and fructose, which were further converted into CQDs in the basic solution [22]. The solution darkened with increasing concentration of the CQDs [23]. The duration of microwave heating markedly affected the properties of the CQDs. Longer microwave exposures enhanced the CQD formation, as evidenced by the corresponding changes in absorption peak position, fluorescence intensity, and color under normal and UV light. XRD analysis revealed that the CQDs featured a crystalline structure with the (002) graphitic plane, while TEM analysis revealed a uniform spherical morphology with a moderately broad size distribution. Enzyme inhibition analysis showed that the CQDs competitively inhibited LDH. Overall, our findings demonstrate the efficiency of the employed method in producing CQDs with controlled structural and optical properties.

Study limitations include the difficulty in controlling synthesis conditions to obtain CQDs with high quantum yields, as the quantum yield is sensitive to even small changes in temperature or reaction time. In addition, sensitive instruments were required for optical measurements, and the results could be affected by changes in parameters such as lighting or contamination.

5. Conclusion

A facile eco-friendly process for producing CQDs from readily available precursors was developed. XRD, TEM, and UV–vis spectroscopy analyses revealed the small size, high crystallinity, and advantageous optical properties of the CQDs. The CQDs exhibited intense fluorescence and high quantum yields and competitively inhibited LDH, thus holding promise for biological and medicinal applications.

Availability of Data and Materials

The datasets used and analyzed during the current study are available from the corresponding author on reasonable request.

Author Contributions

SAN and MAS designed the research study, performed the research and analyzed the data. SMH and ZMH were responsible for data curation, including the organization and validation of experimental results. All authors contributed to the critical revision of the manuscript for important intellectual content. All authors read and approved the final manuscript. All authors have participated sufficiently in the work and agreed to be accountable for all aspects of the work.

Ethics Approval and Consent to Participate

This study was approved by the Institutional Review Board of The General Directorate of Misan Education (Misan, Iraq, Approval No. lab-2025-03). The study was conducted in accordance with the guidelines of the Declaration of Helsinki, and all of the participants provided signed informed consent.

Acknowledgment

Thanks to the Department of Physics, College of Science, University of Misan, Misan, Iraq. Thanks to all the peer reviewers for their opinions and suggestions.

Funding

This research received no external funding.

Conflicts of Interest

The authors declare no conflicts of interest.

References

[1] Farzin MA, Abdoos H. A critical review on quantum dots: From synthesis toward applications in electrochemical biosensors for determination of disease-related biomolecules. Talanta. 2021; 224: 121828. https://doi.org/10.1016/j.talanta.2020.121828

[2] Navid P, Akbari-Hasanjani HR, Akbari-Hasanjani R. A Comprehensive Study of Quantum Dots: Ranging From Synthesis to Applications in Electrochemical Biosensors in the Detection of Biomolecules, Gastrointestinal Diseases, and Electrophysiology. Nano Select. 2025; 6: e70046. https://doi.org/10.1002/nano.70046

[3] Hardman R. A toxicologic review of quantum dots: toxicity depends on physicochemical and environmental factors. Environmental Health Perspectives. 2006; 114: 165–172. https://doi.org/10.1289/ehp.8284

[4] Gulati S, Baul A, Amar A, Wadhwa R, Kumar S, Varma RS. Eco-Friendly and Sustainable Pathways to Photoluminescent Carbon Quantum Dots (CQDs). Nanomaterials (Basel, Switzerland). 2023; 13: 554. https://doi.org/10.3390/nano13030554

[5] Omar MS. Surface structure-based model to calculate thermal and optical properties in nanoscale and quantum dot semiconductors. Physica B: Condensed Matter. 2024; 691: 416328. https://doi.org/10.1016/j.physb.2024.416328

[6] Lim SY, Shen W, Gao Z. Carbon quantum dots and their applications. Chemical Society Reviews. 2015; 44: 362–381. https://doi.org/10.1039/c4cs00269e

[7] Gulucu A, Polat EO. Optically Switchable Fluorescence Enhancement at Critical Interparticle Distances. Advanced Theory and Simulations. 2025; 8: e01134. https://doi.org/10.1002/adts.202501134

[8] Chen Z, Manian A, Widmer-Cooper A, Russo SP, Mulvaney P. Semiconductor Quantum Dots in the Cluster Regime. Chemical Reviews. 2025; 125: 4359–4396. https://doi.org/10.1021/acs.chemrev.4c00967

[9] [9] Tang B, Li B, Sun Y, Li J, Guo Y, Song J, et al. Hot electron lifetime exceeds 300 nanoseconds in quantum dots with high quantum efficiency. arXiv. .2024 https://doi.org/10.48550/arXiv.2410.05818 (preprint)

[10] Li Z, Chen F, Wang L, Shen H, Guo L, Kuang Y, et al. Synthesis and evaluation of ideal core/shell quantum dots with precisely controlled shell growth: nonblinking, single photoluminescence decay channel, and suppressed FRET. Chemistry of Materials. 2018; 30: .3676–3668 https://doi.org/10.1021/acs.chemmater.8b00183

[11] Shen H, Lin Q, Cao W, Yang C, Shewmon NT, Wang H, et al. Efficient and long-lifetime full-color light-emitting diodes using high luminescence quantum yield thick-shell quantum dots. Nanoscale. 2017; 9: 13583–13591. https://doi.org/10.1039/c7nr04953f

[12] Cao L, Meziani MJ, Sahu S, Sun YP. Photoluminescence properties of graphene versus other carbon nanomaterials. Accounts of Chemical Research. 2013; 46: 171–180. https://doi.org/10.1021/ar300128j

[13] Ratre P, Nazeer N, Kumari R, Thareja S, Jain B, Tiwari R, et al. Carbon-Based Fluorescent Nano-Biosensors for the Detection of Cell-Free Circulating MicroRNAs. Biosensors. 2023; 13: 226. https://doi.org/10.3390/bios13020226

[14] Khan AA, Allemailem KS, Alhumaydhi FA, Gowder SJT, Rahmani AH. The Biochemical and Clinical Perspectives of Lactate Dehydrogenase: An Enzyme of Active Metabolism. Endocrine, Metabolic & Immune Disorders Drug Targets. 2020; 20: 855–868. https://doi.org/10.2174/1871530320666191230141110

[15] Wright PC, Qin H, Choi MM, Chiu NH, Jia Z. Carbon nanodots interference with lactate dehydrogenase assay in human monocyte THP-1 cells. SpringerPlus. 2014; 3: 615. https://doi.org/10.1186/2193-1801-3-615

[16] Hernández-Meza JM, Sampedro JG. Trehalose Mediated Inhibition of Lactate Dehydrogenase from Rabbit Muscle. The Application of Kramers' Theory in Enzyme Catalysis. The Journal of Physical Chemistry. B. 2018; 122: 4309–4317. https://doi.org/10.1021/acs.jpcb.8b01656

[17] Williams AT, Winfield SA, Miller JN. Relative fluorescence quantum yields using a computer-controlled luminescence spectrometer. Analyst. 1983; 108: 1067–1071. https://doi.org/10.1039/AN9830801067

[18] Al-Essa K, Al-Essa EM, Qarqaz A, Al-Issa S, Alshahateet SF, Al-Fawares OL. Graphitic carbon nitride/CeO2 nanocomposite for photocatalytic degradation of methyl red. Water. 2025; 17: 158. https://doi.org/10.3390/w17020158

[19] Li S, Mao J. The Influence of Different Types of Graphene on the Lithium Titanate Anode Materials of a Lithium Ion Battery. Journal of Electronic Materials. 2018; 47: .5416–5410 https://doi.org/10.1007/s11664-018-6439-7

[20] Acar Y, Coban MB, Gungor E, Dogan M, Turhan Y. Spectroscopic and morphological properties of white light emitted electrospun PVA@ ZnO: xDy3+ nanofibers. Reactive and Functional Polymers. 2025; 217: 106463. https://doi.org/10.1016/j.reactfunctpolym.2025.106463

[21] Powers KW, Palazuelos M, Moudgil BM, Roberts SM. Characterization of the size, shape, and state of dispersion of nanoparticles for toxicological studies. Nanotoxicology. 2007; 1: 42–51. https://doi.org/10.1080/17435390701314902

[22] Li Y, Zhong X, Rider AE, Furman SA, Ostrikov KK. Fast, energy-efficient synthesis of luminescent carbon quantum dots. Green Chemistry. 2014; 16: 2566–2570. https://doi.org/10.1039/C3GC42562B

[23] Tang L, Ji R, Cao X, Lin J, Jiang H, Li X, et al. Deep ultraviolet photoluminescence of water-soluble self-passivated graphene quantum dots. ACS Nano. 2012; 6: 5102–5110. https://doi.org/10.1021/nn300760g